Method-of-moments analysis of narrow-wall slot array in a rectangular waveguide

Article *in* IEE Proceedings - Microwaves Antennas and Propagation · July 2000

DOI: 10.1049/ip-map:20000261 · Source: IEEE Xplore

3 authors:

Vaidya Shikha Prakash
Padaav Speciality Ayurvedic Treatment Center
51 PUBLICATIONS **2,458** CITATIONS
SEE PROFILE

Somita Christopher
CARE Hospitals
26 PUBLICATIONS **68** CITATIONS
SEE PROFILE

Narayanaswamy Balakrishnan
Indian Institute of Science
209 PUBLICATIONS **2,351** CITATIONS
SEE PROFILE

Method-of-moments analysis of the narrow-wall slot array in a rectangular waveguide

V.V.S.Prakash, S.Christopher and N.Balakrishnan

Abstract: The method-of-moments has been used for the analysis of the nonresonant narrow-wall slot array in a rectangular waveguide. As this approach works with the fundamental integral equations that describe the entire array, no assumptions about the aperture electric fields are required. Also, the equivalent circuit representation for the individual radiating slots used in earlier designs is not required in the present method, as it deals directly with slot aperture voltages. The effects of internal higher-order and external mutual couplings, and finite wall thickness are rigorously incorporated in the design. Expressions are presented for the input reflection coefficient, transmission coefficient, and the far-field radiation pattern of the array. Numerical results are compared with the experimental results of a 78 element narrow-wall slot array. Good agreement has been observed between theory and experiment.

1 Introduction

Waveguide slotted arrays are ideally suited for the generation of low-sidelobe far-field patterns and are preferred in several strategic applications. Every point in the distribution is individually determined by slot location and shape, and these can be readily milled with precision. The theoretical analysis and design tools are well developed and readily available in the open literature for broad-wall slot arrays [1–7]. In 1978, Elliot and Kurtz [1] developed a design procedure that would permit determination of the length and offset of each slot in a linear/planar array of longitudinal broad-wall slots once the desired pattern and input admittance were specified. They presented an expression for the active admittance of the slot in terms of slot voltages and self and mutual admittances. Following a similar approach they developed a design approach for nonresonantly spaced broad-wall longitudinal slots [2] and waveguide-fed series slot array [3]. In 1983, an improved version of their design procedure was presented [4] and then in 1986, Elliot and O'Loughlin [5] indicated how TE_{20} internal mutual coupling could be approximated and folded into the design formulas. Elliot's procedure uses the characterisation data of isolated slot. Elliot assumed that the electric field in each slot is represented by a single sinusoid, with the slot discontinuity represented by a shunt element on an equivalent transmission line. Even though the effect of finite waveguide wall thickness is rigorously incorporated in analysing the isolated slot, its effect is neglected in the design of a slotted array. Gulick [6] presented a design approach for linear and planar arrays of waveguide-fed broad-wall longitudinal slots using the method of moments (MoM). Sangster and McCormick [7] presented a theoretical design and synthesis of shunt slots on the broad-wall of a rectangular waveguide.

The majority of the literature focused on the broad-wall longitudinal offset slot arrays. A rigorous narrow-wall slot array design methodology is not available in the open literature, but the characterisation of the individual radiating element and the mutual coupling effects have been extensively studied by Prakash *et al.* [8–10]. Dion [12] presented a continuous aperture model for the design of nonresonant slot arrays. He presented an in-depth analysis on the beam scanning, power leakage, etc. A comprehensive review of the literature on waveguide slots and arrays has been presented by Rengarajan *et al.* [13].

This paper presents a MoM-based analysis of the nonresonant narrow-wall inclined slot arrays. Since the fundamental integral equations that describe the array are used directly, no assumptions about the nature of the aperture fields are required. The internal mutual coupling between the slots to an arbitrary number of higher-order modes is included, and the waveguide wall thickness is accounted for rigorously. Expressions are presented for the input reflection coefficient, transmission coefficient, and the far-field radiation pattern of the array. The numerical results are compared with the experimental results of a 78 element narrow-wall slot array. Good agreement has been observed between the theory and the experiment.

2 Theory

Consider the schematic diagram of the narrow-wall slot array shown in Fig. 1. All the slots are uniformly spaced with an interslot spacing denoted by d. Successive slots are alternatively tilted to give the required phase progression across the array aperture. The waveguide wall thickness is finite and the array is fed at one end by a matched generator with TE_{10} mode. A matched load terminates the other end of the array, and this establishes a travelling wave inside the waveguide. This type of array is also known as a

IEE Proceedings online no. 20000261

DOI: 10.1049/ip-map:20000261

Paper first received 24th August and in revised form 23rd December 1999

V.V.S. Prakash and S. Christopher are with the Electronics and Radar Development Establishment, Bangalore, India

N. Balakrishnan is with the Indian Institute of Science, Bangalore, India

nonresonant array. The cross-sectional dimensions of the waveguide are chosen such that the only propagating mode is the TE_{10} mode and all higher-order modes are cut off at the operating frequency. Let there be N slots in the array, with the slot closest to the load designated as Nth slot and that closest to the input end as the first slot.

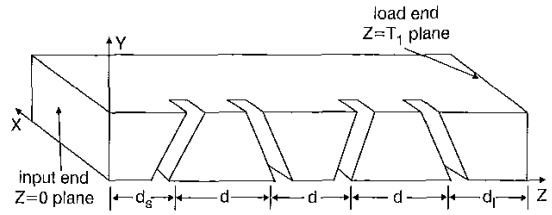

Fig. 1 *Schematic diagram of narrow-wall slot linear array*

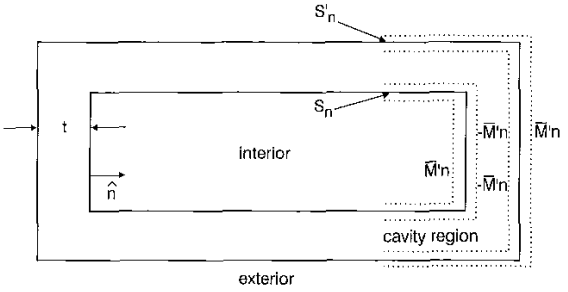

Fig. 2 *Placement of equivalent magnetic current densities for typical nth slot in array*

2.1 Coupled integral equations

As a result of TE_{10} mode excitation at the input end of the array, an electric field is established at the interior and the exterior apertures of each of the slots. Using the equivalence principle, the interior and the exterior apertures of each of the slots are closed by a perfect electric conductor and equivalent magnetic current densities are placed at the shorted apertures as shown in Fig. 2. The unit tangential vectors to the interior and exterior surfaces directed along the slot centre are denoted by $\bar{S}_n$ and $\bar{S}'_n$, respectively. The magnetic current densities on the interior and exterior apertures are denoted by $\bar{M}_n$ and $\bar{M}'_n$, respectively.

A set of coupled integral equations are obtained for the nth slot by equating the total tangential magnetic field available on either side of the interior and exterior apertures.

$$\left[\bar{H}_n^{int}(\bar{M}_n) + \sum_{\substack{q=1 \\ q\neq n}}^{N} \bar{H}_n^{int}(\bar{M}_q) + \bar{H}_{10,n}^{inc}\right].\hat{S}_n = \left[\bar{H}_n^{c}(-\bar{M}_n) + \bar{H}_n^{c}(-\bar{M}'_n)\right].\hat{S}_n \quad (1)$$

at aperture S_n

$$\left[\bar{H}_n^{c}(-\bar{M}_n) + \bar{H}_n^{c}(-\bar{M}'_n)\right].\hat{S}'_n = \left[\bar{H}_n^{ext}(\bar{M}'_n) + \sum_{\substack{q=1 \\ q\neq n}}^{N} \bar{H}_n^{ext}(\bar{M}'_q)\right].\hat{S}'_n \quad (2)$$

at aperture S'_n

for all $n = 1, 2, ..., N-1, N$, where $\bar{H}_n^{int}$ internal scattered magnetic field, $\bar{H}_n^{ext}$ is the external scattered magnetic field, $\bar{H}_n^{c}$ is the cavity scattered magnetic field, $\bar{H}_{10,n}^{inc}$ is the incident TE_{10} magnetic field, and the subscript n stands for the slot number. The two equations have to be satisfied simultaneously for all the N slots in the array.

2.2 Method of moments solution

The coupled integral equations (eqns. 1 and 2) are formulated for all the slots, and are solved using MoM. At the interior and the exterior apertures of the nth slot, the magnetic current densities are expanded as

$$\bar{M}_n = \sum_{j=1}^{M} \alpha_j^n \bar{f}_j^n \quad (3)$$

$$\bar{M}'_n = \sum_{j=1}^{M} \alpha_j'^n \bar{f}_j'^n \quad (4)$$

where α_j^n and $\alpha_j'^n$ are the unknown complex constants at the interior and exterior apertures of nth slot corresponding to the jth basis function, respectively, and $\bar{f}_j^n$ and $\bar{f}_j'^n$ are the known vector basis functions. For each slot in the array, eqns. 1 and 2 represent a linear system of $2M$ algebraic equations in terms of the unknown complex expansion coefficients α and α', as seen from eqns. 3 and 4. For an array of N slots, a system of $2MN$ equations is obtained. For the entire array these equations are formulated, rearranged and put in a matrix form $[\boldsymbol{Y}]\,[\boldsymbol{x}] = [\boldsymbol{h}]$ where $[\boldsymbol{Y}]$ is the known matrix of $2MN \times 2MN$, $[\boldsymbol{x}]$ is the unknown coefficient matrix of $2MN \times 1$ and $[\boldsymbol{h}]$ is the known excitation matrix of $2MN \times 1$ in size. The resulting matrix equation is given by

$$\begin{bmatrix} [\boldsymbol{Y}^{11}] & [\boldsymbol{Y}^{12}] & [\boldsymbol{Y}^{13}] & \cdots & [\boldsymbol{Y}^{1N}] \\ [\boldsymbol{Y}^{21}] & [\boldsymbol{Y}^{22}] & [\boldsymbol{Y}^{23}] & \cdots & [\boldsymbol{Y}^{2N}] \\ [\boldsymbol{Y}^{31}] & [\boldsymbol{Y}^{32}] & [\boldsymbol{Y}^{33}] & \cdots & [\boldsymbol{Y}^{3N}] \\ \cdots & \cdots & \cdots & \cdots & \cdots \\ \cdots & \cdots & \cdots & \cdots & \cdots \\ [\boldsymbol{Y}^{N1}] & [\boldsymbol{Y}^{N2}] & [\boldsymbol{Y}^{N3}] & \cdots & [\boldsymbol{Y}^{NN}] \end{bmatrix} \times \begin{bmatrix} [\boldsymbol{x}^{(1)}] \\ [\boldsymbol{x}^{(2)}] \\ [\boldsymbol{x}^{(3)}] \\ \cdots \\ \cdots \\ [\boldsymbol{x}^{(N)}] \end{bmatrix} = \begin{bmatrix} [\boldsymbol{h}^{(1)}] \\ [\boldsymbol{h}^{(2)}] \\ [\boldsymbol{h}^{(3)}] \\ \cdots \\ \cdots \\ [\boldsymbol{h}^{(N)}] \end{bmatrix} \quad (5)$$

Each submatrix $[\boldsymbol{Y}^{pq}]$ for $p, q = 1, 2, ..., N-1, N$, is of size $2M \times 2M$, and the vector $[\boldsymbol{x}^{(p)}]$ is the unknown matrix of size $2M \times 1$. The vector $[\boldsymbol{h}^{(p)}]$ is the excitation matrix of size $2M \times 1$. Each row of the coefficient matrix in eqn. 5 represents the result of the inner product between the weighting functions and the scattered magnetic field at that particular slot. The diagonal submatrices of $[\boldsymbol{Y}]$ represent the interactions at a given slot due to the source at the same slot, namely self-reaction. The off-diagonal submatrices account for the coupling effects from all other slots in the waveguide. The evaluation of the submatrix $[\boldsymbol{Y}^{pp}]$ involves only the self-reaction of the pth slot and does not include the other slots. This matrix is exactly the same as the admittance matrix derived for the isolated narrow-wall slot in [8].

The off-diagonal submatrices of the admittance matrix $[\boldsymbol{Y}]$ are given by

$$[\boldsymbol{Y}^{pq}] = \begin{bmatrix} [\boldsymbol{Y}^{11,pq}] & [0] \\ [0] & [\boldsymbol{Y}^{22,pq}] \end{bmatrix} \quad \text{for } p \neq q \quad (6)$$

where $Y_{ij}^{11,pq}$ denotes the internal mutual coupling between the slot p and slot q, $Y_{ij}^{22,pq}$ denotes the external mutual

coupling, and the matrix [0] is the null vector. The evaluation of the internal mutual coupling is carried out using the spectral domain waveguide Green's function [8, 9]. To demonstrate the significance of higher-order internal mutual coupling, a test case is taken up with two slots cut on a WR90 waveguide with same tilts and lengths of 15° and $0.55\lambda_0$, respectively, at 9.375GHz. The distance between the two slots is varied from 0.25 to $2\lambda_g$ for the purpose of the study. The contribution of the first four higher-order modes to the internal coupling matrix element is computed with respect to that of TE_{10} dominant mode and the values are plotted in Fig. 3. When the slots are separated by more than $0.7\lambda_g$, the contribution of all higher-order modes falls off to as low as 10^{-5} of that of the dominant mode. For slot separations less than λ_g, the TE_{01}- and TE_{11}-mode contributions are significant than that of TE_{20} mode. In view of these data, the higher-order mode coupling between two edge slots inside the waveguide need to be considered for successive slots only i.e. $|p - q| = 1$. Also for any two successive slots, only the first three higher-order modes, namely TE_{20}, TE_{01}, and TE_{11}, contribute significantly to the internal coupling matrix. The external scattered fields are evaluated using S2DS technique, identical to that employed by Prakash, *et al.* [8–10].

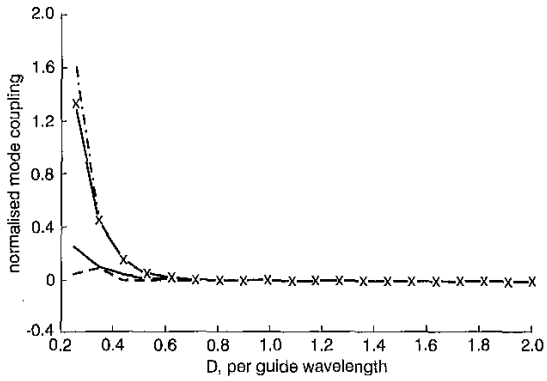

Fig. 3 $|Y_{ij}^{11,pq}|$ *against slot spacing*
$\theta_p = \theta_q = 15°$, $2L'_p = 2L'_q = 0.55\lambda_0$ at 9.375 GHz for p = q = 1
TE20/TE10
TE01/TE10
TE11/TE10
TE30/TE10

Given a nonresonant array of N inclined narrow-wall slots, eqn. 5 is formulated, and the interior and the exterior aperture fields at each of the slots in the array are then computed by solving this equation.

2.3 Array reflection and transmission coefficients

The reflection and transmission coefficients of the array are computed from the equivalent magnetic current densities at the slot apertures. In Fig. 1, the reference plane for the z-co-ordinate coincides with the plane where the input flange is connected and is away from the centre line of the first slot by d_s. The input reflection coefficient is defined with respect to the dominant TE_{10} mode of propagation inside the waveguide as

$$\Gamma_{10} = \frac{-\pi}{\omega\mu_0 a^2 b\beta_{10}} \sum_{q=1}^{N}\sum_{j=1}^{M} \alpha_j^q \left[\beta_{10} I_x^{j,q}(0) - j\sin\theta_q \left(\frac{\pi}{a}\right) I_z^{j,q}(0)\right] \tag{7}$$

The transmission coefficient of the array is defined with respect to the dominant TE_{10} mode at the output of the array ($z = T_1$ plane) as

$$T_{10}^t\big|_{z=T_1} = 1 - \frac{\pi}{\omega\mu_0 a^2 b\beta_{10}} \sum_{q=1}^{N}\sum_{j=1}^{M} \alpha_j^q \times \left[-\beta_{10} I_x^{j,q}(T_1) - j\sin\theta_q \left(\frac{\pi}{a}\right) I_z^{j,q}(T_1)\right] e^{j\beta_{10}T_1} \tag{8}$$

where ω is the angular frequency, μ_0 is the free-space permittivity, β_{10} is the TE_{10} mode phase constant. The parameters $I_x^{j,q}$ and $I_z^{j,q}$ are given by

$$I_x^{j,q}(z) = \int_{x'=a-\delta_q}^{a}\int_{z'=z_c^b-w'/2}^{z_c^b+w'/2} S_{x'} \sin\left[\frac{j\pi}{2L_q}(\delta_q - a + x')\right] \times e^{-\Gamma_{10}|z-z'|}dx'dz' \tag{9}$$

$$I_z^{j,q}(z) = \iint_{y'\,z'} \sin\left[\frac{j\pi}{2L_q}(\eta' + L_q)\right] e^{-\Gamma_{10}|z-z'|}dy'dz' \tag{10}$$

and

$$S_{x'} = \sin\left(\frac{\pi x'}{a}\right) \tag{11}$$

$$z_c^b = z_q + L_{1,q}\sin\theta_q$$
$$z_c^t = z_q - L_{1,q}\sin\theta_q \tag{12}$$

where Γ_{10} is the TE_{10} mode propagation constant, w' is the slot width, δ_q and L_q are the depth of cut and length of slot q, respectively, a and b are the broad- and narrow-wall dimensions of the waveguide, respectively, and z_q is the z-co-ordinate of the centre of the qth slot. The radiated field for a linear array of N radiators with uniform spacing of d can be expressed as the product of the element factor and the array factor. Since the element factor is a slowly varying function of θ and ϕ and is very broad in nature, all the fine structure in the radiation pattern comes from the array factor. Under this approximation, the radiated field of the array is given by

$$F(\phi) = \sum_{n=1}^{N}\sum_{i=1}^{M} \alpha_i'^n \sin\left[\frac{i\pi}{2}\right] e^{-jk_0 d\cos\phi} \tag{13}$$

where ϕ is measured with respect to the array axis.

3 Results

To validate the MoM formulation presented in the previous Sections, the S_{11}, S_{21} and the far-field patterns of a 78 element sidewall inclined-slot nonresonant array have been computed. This readily available experimental 78 element array was originally designed at 9.05GHz using Dion's method [11], with a beam squint of 0.8° away from the antenna boresight, and tilted towards the load end. The interelement spacing is 2.456cm. The slot width is 2.5mm and all the slots are taken to be of same width. A spacing of 5.02cm is left at the input end for connecting the flange and 3.11cm is left at load end for connecting a push-fit matched load. The total length of the array, including the input/output spacing, becomes 1.973m. The inclinations

and depth of cuts on the broadwall of each of the slots in the array are presented in Fig. 4.

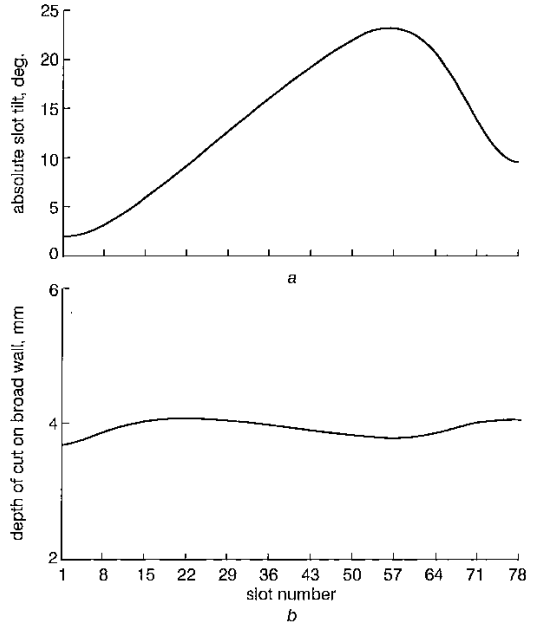

Fig. 4 *Slot tilt and depth of cut against slot number for 78 element array*
a Slot tilt
b Depth of cut

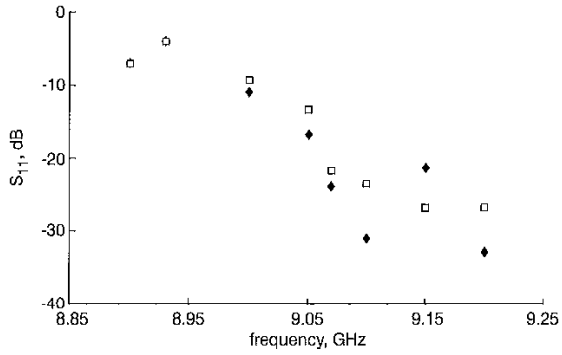

Fig. 5 *Reflection coefficient against frequency of narrow-wall slot array*
◆ experimental
□ simulated

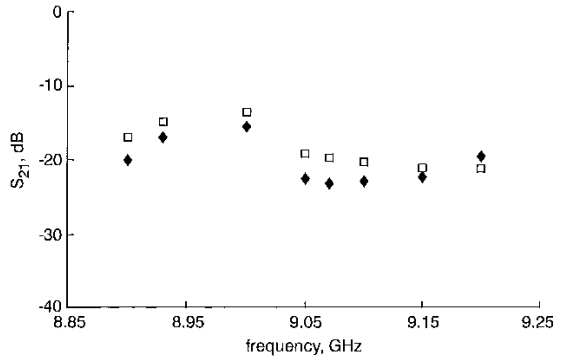

Fig. 6 *Transmission coefficient against frequency of narrow-wall slot array*
◆ experimental
□ simulated

Using these nonresonant array parameters and slot inclinations and depth of cuts on the broadwall of the array given in Fig. 4, the S_{11} and S_{21} of the array have been computed at a set of discrete frequency spots using the MoM analysis and presented in Figs. 5 and 6. These parameters of the array are also measured with a HP8510B vector network analyser, sampled at the same set of frequency spots and presented in Figs. 5 and 6 for comparison. The S-parameters as a function of frequency exhibit similar trend for both the theoretical and experimental data. The computed S_{11} reaches a high value of –4.195dB at 8.93GHz, while the measured value is –3.9dB at the same frequency. Also, the computed S_{21} is –14.86dB while the measured value is –16.9dB at 8.93GHz. The discrepancy between the theory and experiment could be attributed to various mechanical aspects like the machining errors in slot tilt, depth of cut, nonuniformity of interslot spacing, etc. Also, the array is nearly 2m in length and any slight bow in the array would get magnified from one end to the other. In view of these mechanical limitations it is seen that good agreement is obtained between the simulated data and experimental values over the band of frequencies.

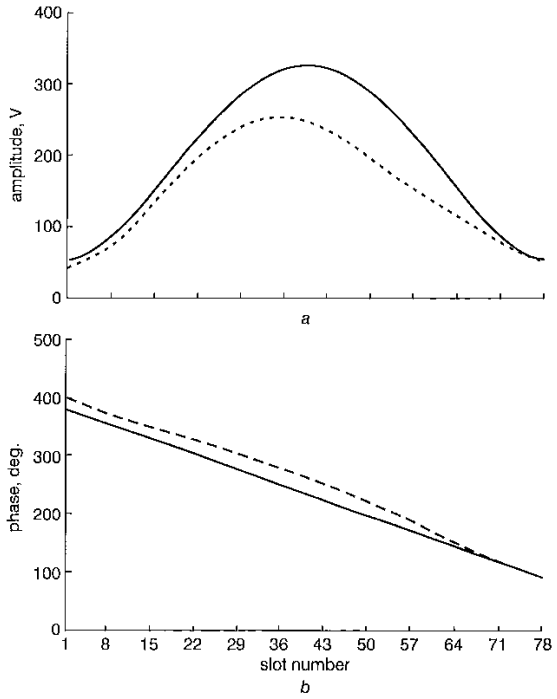

Fig. 7 *Aperture distribution of 78 element array computed using MoM analysis at 9.05GHz*
a Amplitude
– – Taylor –35dB distribution
····· MoM analysis
b Phase
– – linear phase progression
····· MoM analysis

A plot of the aperture amplitude and phase distribution of the array computed using the MoM analysis at 9.05GHz is presented in Fig. 7. The aperture excitation for which the array was originally designed is also presented. The MoM analysis showed that the amplitude distribution of the array is asymmetrical and the aperture phase instead of being linearly progressive, has an error component superimposed on it. One of the critical parameter is the far-field pattern of the array. This pattern has been computed using the MoM analysis and is shown in Fig. 8 along with the measured pattern at 9.05GHz. The measurement of the array has been carried out in an open test range [14], with the test antenna mounted on a three-axis positioner (capacity of 1 tonne) at the receiving end. The three-axis positioner can hold a planar antenna of more than 3m height and 7m in length. The elevation can rotate from +45 to

–90°, the top azimuth has 360° continuous rotation, and the bottom azimuth has ±240° rotation. The open test range has 1.6km separation between the transmitter and receiver. The receiver is Scientific Atlanta 1783SA and the pattern recorder is 1580SA. The transmitting antenna is a parabolic reflector, with a Scientific Atlanta synthesised source 2180SA. In Fig. 8, each major division along the horizontal axis corresponds to 5°, and that along the vertical axis corresponds to 2dB. This amounts to a scaling of 0 to –40dB along vertical axis and ±45° along horizontal axis. There is good agreement between the results computed using the MoM analysis and the experimental results. The dominant feature of the pattern is a shoulder/kink in the right side of the mainbeam. This turns out to be at –18.59dB level at +1.53° away from the main beam as predicted by theory. From the experimental results of Fig. 8, this shoulder/kink is at –18.4dB level at +1.9° from the mainbeam. The first peak left sidelobe and right sidelobe levels are found to be –27.06 and –28.23dB, respectively; while the experimental data shows a –27 and –25.8dB left and right sidelobe levels. Except for the first few sidelobes, all other sidelobe peaks are below –30dB which is also the case for the simulated far-field pattern. The experimental and theoretical half-power beamwidths are 1.45 and 1.2°, respectively.

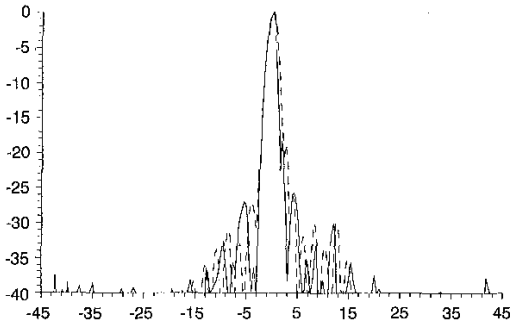

Fig. 8 *Far-field patterns of narrow-wall slot array at 9.05 GHz*
x-axis ±45°; *y*-axis –40dB
– – – – simulated
–·–·– measured

Good agreement is found between the measured electrical characteristics and the theoretical computed data. Certain errors like the machining errors, measurement errors, etc. influence the array performance strongly and are extremely difficult to model. Also, modelling large arrays is computationally complex and the growing numerical errors would limit realisable accuracy. In view of these limitations, it can be said that the MoM-based approach presented here can predict the electrical characteristics of the narrow-wall inclined slot array with a reasonably good accuracy. Given a linear array of narrow-wall slot radiators cut on a rectangular waveguide, the performance of the array can be judged using the present analysis *a priori*, instead of resorting to a time-consuming and costlier process of fabrication and testing.

4 Conclusion

A MoM-based formulation has been presented for the analysis of waveguide-fed narrow-wall slot arrays. As this approach works with the fundamental integral equations that describe the entire array, no assumptions about the aperture electric fields are required. Also, the equivalent circuit representation for narrow-wall slots used in the earlier designs is not required, as it deals directly with slot aperture voltages. The effects of the internal higher-order and the external mutual couplings, and the finite wall thickness are rigorously incorporated in the design. Theoretical derivations are presented for the performance evaluation of the array, namely, the input reflection coefficient, transmission coefficient, far-field patterns, aperture voltages, etc. The theoretical formulation has been validated by comparison with the experiments. This MoM-based analysis is completely general and can be extended to resonant slot arrays, arrays with nonuniformly spaced slots, etc.

5 References

1 ELLIOTT, R.S., and KURTZ, L.A.: 'The design of small slot arrays', *IEEE Trans.*, 1978, **AP–26**, pp. 214–219
2 ELLIOTT, R.S.: 'On the design of travelling-wave-fed longitudinal shunt slot arrays', *IEEE Trans.*, 1979, **AP–27**, pp. 717–720
3 OREFICE, M., and ELLIOTT, R.S.: 'Design of waveguide-fed series slot arrays', *IEE Proc.-H*, 1982, **129**, pp. 165–169
4 ELLIOTT, R.S.: 'An improved design procedure for small arrays of shunt slots', *IEEE Trans.*, 1983, **AP–31**, pp. 48–53
5 ELLIOTT, R.S., and O'LOUGHLIN, W.R.: 'The design of slot arrays including internal mutual coupling', *IEEE Trans.*, 1986, **AP–34**, pp. 1149–1154
6 GULICK, J.J.: 'The design of linear and planar arrays of waveguide-fed longitudinal slots'. PhD Dissertation, University of California, Los Angeles, June 1987
7 SANGSTER, S.J., and MCCORMICK, A.H.I.: 'Theoretical design/synthesis of slotted waveguide arrays', *IEE Proc.-H*, 1989, **136**, pp. 39–46
8 PRAKASH, V.V.S., CHRISTOPHER, S., and BALAKRISHNAN, N.: 'Sidewall inclined slot in a rectangular waveguide: Theory and experiment', *IEE Proc.-H*, 1998, **145**, (3), pp. 233–238
9 PRAKASH, V.V.S., CHRISTOPHER, S., and BALAKRISHNAN, N.: 'Hybrid method of analysis of slot discontinuity in a rectangular waveguide and the validity of circuit representation', *Int. J. RF Microw. CAE*, 1998, **8**, pp. 339–349
10 PRAKASH, V.V.S., CHRISTOPHER, S., and BALAKRISHNAN, N.: 'Mutual coupling between edge slots on a rectangular waveguide'. Presented at the National symposium on *Microwave and light waves*, New Delhi, India, March 1998
11 PRAKASH, V.V.S., CHRISTOPHER, S., and BALAKRISHNAN, N.: 'On the application of Fourier transform techniques to waveguide interior regions', *J. SEE Electrotechnol., India*, 1996, **40**, (3/4), pp. 42–50
12 DION, A.: 'Nonresonant slotted arrays', *IRE Trans.*, 1958, **AP–6**, pp. 360–365
13 RENGARAJAN, S.R., JOSEFSSON, L.G., and ELLIOT, R.S.: 'Waveguide-fed slot antennas and arrays: A review', *Electromagn.*, 1999, **19**, (1), pp. 3–22
14 CHRISTOPHER, S., PRAKASH, V.V.S., and ABID HUSSAIN, V.A.: 'Planar elliptical nonresonant array for airborne radar applications', *IETE Tech. Rev.*, 1999, **16**, (2), pp. 145–150